Available online at www.sciencedirect.com
ScienceDirect
Catalysis Today 129 (2007) 336–345
CATALYSIS TODAY
www.elsevier.com/locate/cattod

Ethanol steam reforming over Ni/La–Al_2O_3 catalysts: Influence of lanthanum loading

M.C. Sánchez-Sánchez, R.M. Navarro *, J.L.G. Fierro

Instituto de Catálisis y Petroleoquímica, CSIC, C/Marie Curie 2, Cantoblanco 28049, Madrid, Spain

Available online 24 October 2007

Abstract

Hydrogen production from ethanol reforming over nickel catalysts supported on lanthanum loaded Al_2O_3 substrates was studied. Activity results revealed the enhancement in the reforming stability of the Ni catalysts with the increase in the lanthanum loading on Al_2O_3 substrates. Catalytic behavior of Ni/La–Al_2O_3 catalysts in the ethanol steam reforming was found to be the contribution of the activity of the La–Al_2O_3 supports for the ethanol dehydration reaction and the activity of the nickel metallic phase that catalyzes both dehydrogenation and C–C bond rupture. Physicochemical characterization of catalysts revealed that acidity, nickel dispersion and nickel-support interaction depend on the La-loading on Al_2O_3. The better reforming stability of catalysts with the increase in La content was explained in terms of the ability of nickel surface and/or La–Ni interactions to prevent the formation of carbon filaments.

Keywords: Ethanol; Hydrogen production; Nickel catalyst; Steam reforming; Al_2O_3; Lanthanum

1. Introduction

The scarcity of fossil fuels and the pollution problems associated with their use have attracted the attention of the scientific, governmental and industrial communities towards the search for alternative energy systems. Among all alternatives, hydrogen is an excellent vector when used directly as a fuel in internal combustion engines or, indirectly to supply electricity using fuel-cells. The production of hydrogen from biomass is receiving increased attention as a potential source of renewable energy respect to global issues of sustainable energy. In this context, the ethanol may represent a potential source for hydrogen production. Ethanol can be efficiently converted in hydrogen by means of its catalytic reaction with steam according to the following reaction:

$$CH_3CH_2OH + 3H_2O \rightarrow 6H_2 + 2CO_2, \quad \Delta H^\circ = 207.7\,\text{kJ/mol} \qquad (1)$$

Ethanol-reforming reactions include several catalytic steps such as: (i) ethanol dehydrogenation, (ii) carbon–carbon bond breaking of surface intermediates to produce CO and CH_4 and, (iii) water reforming of the C_1 intermediate products to generate hydrogen. On the basis of the influence of the nature of both the metal and support on the catalytic characteristics of supported metals, choice of these elements is a key factor to developing supported catalysts that fulfil the above requirements. According to the literature, different metals (Ni [1], Co [2,3], Ni–Cu [4], Pt, Pd, Rh [5–8] deposited on oxide supports (Al_2O_3, La_2O_3, ZnO, MgO, etc.) have shown to be active in the ethanol-reforming reaction. Among transition metals, the high C–C bond-breaking activity and the relatively low cost of Ni make it a suitable active phase for ethanol-reforming reactions. The nature of support strongly influences the catalytic performance of supported Ni catalyst for the steam reforming of ethanol since it affects dispersion and stability of the metal as well as it may participate in the reaction. Among oxide supports, alumina-based supports are often used in reforming catalysts because of their mechanical and chemical resistance under reaction conditions. Nevertheless the use of Al_2O_3 as support promotes catalysts deactivation by deposition of carbon from the ethylene intermediate produced via dehydration reactions of ethanol on acid sites of the support. Thus basic neutral or basic oxides are preferred as support in catalyst formulations applied to ethanol reforming. Among these, Ni dispersed on La_2O_3 is know to be an excellent formulation for steam reforming of ethanol taking into account its high activity,

* Corresponding author. Tel.: +34 915854773; fax: +34 915854760.
E-mail address: r.navarro@icp.csic.es (R.M. Navarro).

0920-5861/$ – see front matter © 2007 Elsevier B.V. All rights reserved.
doi:10.1016/j.cattod.2006.10.013

selectivity and stability even under conditions whose favours carbon formation [1,6,9]. The beneficial effect of lanthanum oxide in the stability of Ni-based catalysts have been attributed to scavenging of coke deposition on nickel surface by lanthanum oxycarbonate species that are developed on the top of Ni particles or at the Ni–La interface under reaction conditions [1]. From a practical point of view, and in order to maximize the exposed surface of nickel and lanthanum both elements are added to a high-surface area substrates such as Al_2O_3.

With this background, the aim of the present work was to study the effect of adding different amounts of lanthana on alumina support on the behavior of Ni catalysts in the production of hydrogen by steam reforming of ethanol. Careful investigations of the structure of the catalysts were performed in an attempt to understand the relationship between activity and their structural and surface characteristics.

2. Experimental

2.1. Supports and catalysts preparation

La–Al_2O_3 supports were prepared by incipient wetness pore volume impregnation of a commercial γ-Al_2O_3 (Alfa Aesar, S_{BET} = 212 m^2/g) with an aqueous solution of lanthanum nitrate ($La(NO_3)_3{\cdot}6H_2O$ 99.9% Johnson Matthey). After impregnation, the supports were dried under air at 393 K for 3 h and subsequently calcined in air at 923 K for 6 h. La_2O_3 loadings in the different supports (3, 6 and 15 wt%) were selected in order to achieve 0.08, 0.16 and 0.40 theoretical monolayers of La_2O_3 on Al_2O_3, respectively. The supports were referred to hereafter as AxL where x refers to the lanthanum oxide loading (3, 6, 15 wt%) added to Al_2O_3 carrier.

Supported Ni catalysts were prepared by impregnation of each of the above supports using aqueous solutions of $Ni(NO_3)_2$ at 333 K under stirring. Ni-loading in the different catalysts was selected in order to achieve 0.75 theoretical monolayers over supports. After Ni incorporation, the samples were dried at 393 K for 2 h and subsequently calcined in air at 773 K for 4 h. The catalysts were labelled as Ni/AxL following the same designation previously described for the supports. A sample supported on bare Al_2O_3 (Ni/A) was also prepared as reference catalyst.

2.2. Catalyst characterization

Elemental analyses were performed by inductively coupled plasma atomic emission spectroscopy (ICP-AES) on a Perkin-Elmer Optima 3300 DV device. Samples were first dissolved in acidic solutions (mixture of HF, HCl, HNO_3 and H_3PO_4), micro-waved for 1 h and diluted to concentrations within the calibration range of the instrument. Oxides content in calcined samples (Table 1) were calculated from metal percentages determined by ICP assuming dry samples and NiO, La_2O_3 and Al_2O_3 as the oxides species presents in the calcined state.

The specific surface areas of the catalysts were calculated by applying the BET method to the N_2 adsorption isotherms, measured at liquid nitrogen temperature on a Micromeritics ASAP 2100 apparatus on samples previously degassed at 473 K for 24 h.

Table 1
Chemical composition (wt%) of calcined catalysts

	NiO	La_2O_3	Al_2O_3
Ni/A	16.0	–	Balance
Ni/A3L	15.9	2.9	Balance
Ni/A6L	16.0	5.8	Balance
Ni/A15L	16.2	14.6	Balance

FTIR spectra of adsorbed pyridine were recorded with a Nicolet 5ZDX Fourier transform spectrophotometer, working with a resolution of 4 cm^{-1} over the entire spectral range and averaged over 100 scans. The samples, in the form of self-supporting wafers (thickness ca. 10 mg/cm^2), were degassed at 673 K for 1 h. After admission of pyridine (1.5 mbar for 15 min) spectra were recorded after degassing for 30 min at 423, 523 and 623 K.

X-ray diffraction patterns were recorded on calcined supports and reduced catalysts using a Seifert 3000 P vertical diffractometer and nickel-filtered Cu Kα radiation (λ = 0.1538 nm) under constant instrument parameters. Reduction of samples was carried out *ex situ* in a tubular flow reactor (923 K in H_2/N_2 (1/9 vol) and the samples protected under *iso*-octane before being transferred into the instrument. For each sample Bragg angles between 5° and 80° were scanned. A rate of 5 s/step (step size: 0.04° 2θ) was used during a continuous scan in the above-mentioned range. Volume-averaged crystallite sizes were determined by applying the Debye–Scherrer equation.

Temperature-programmed reduction experiments were carried out with a semiautomatic Micromeritics TPD/TPR 2900 apparatus equipped with a TC detector. Prior to reduction experiments, the samples, about 30 mg, were thermally treated under air stream at 573 K to remove water and other contaminants. TPR profiles were obtained by heating the samples under a 10% H_2/Ar flow (50 mL/min) from 298 to 1173 K at a linearly programmed rate of 10 K/min.

X-ray photoelectron spectroscopy (XPS) was used to study both chemical composition and oxidation state of the catalyst surfaces. Photoelectron spectra were recorded with a VG Escalab 200R electron spectrometer equipped with a Mg Kα X-ray source ($h\nu$ = 1253.6 eV) and a hemispherical electron analyser operating at constant transmission energy (50 eV). The reduction treatment was carried out *ex situ* at 923 K in H_2/N_2 (1/9 vol) flow for 90 min and the samples protected under *iso*-octane before being transferred into the instrument where a second reduction treatment *in situ* at 773 K for 30 min was done. The C 1s, Al 2p, La 3d, Ce 3d and Ni 2p core-level spectra were recorded and the corresponding binding energies were referenced to the C 1s line at 284.6 eV (accuracy within ± 0.1 eV). Due to the partial overlapping of La $3d_{5/2}$ and Ni $2p_{3/2}$ signals, the chemical state of nickel element in Ni/A-L catalyst was elucidated after carefully subtraction of La $3d_{5/2}$ peak from the experimental (Ni 2p + La $3d_{3/2}$) spectrum.

Nickel dispersion on reduced samples was measured by H_2-pulse chemisorption at 298 K using an Ar flow of 50 mL/min

and pulses of 0.1 mL (10% H_2 in Ar) on a Micromeritics ASAP 2100 unit. Prior to pulse chemisorption experiment, all samples were reduced *in situ* under H_2/Ar flow (50 mL/min) for 1 h at 923 K and subsequently flushed under Ar for 15 min at 15 K above the reduction temperature. To calculate metal dispersion, an adsorption stoichiometry of H/Ni = 1 was assumed [12].

Temperature-programmed oxidation analyses of used catalysts were carried out using a thermo-gravimetric analyzer (Mettler Toledo TGA/SDTA 851e) to determine the amount of coke deposited on catalysts. The standard protocol involved the weight change of the sample (20 mg) during its heating in 200 mL/min of N_2 as purge gas and 50 mL/min of O_2 as reactive gas from 298 to 1373 K at a heating rate of 5 K/min.

2.3. Activity tests

Activity tests were performed using 0.1 g of catalyst diluted with SiC (both in the 0.4–0.5 mm particle size range and selected after preliminary mass transport experiments to minimize diffusional resistances) at a volume ratio of 3:1 to avoid adverse thermal effects. The catalyst bed was placed in a 6 mm ID quartz tubular reactor with a coaxially centred thermocouple. Prior to reaction, the catalysts were flushed in nitrogen at 473 K, followed by reduction *in situ* at 923 K for 2 h (heating rate 5 K/min) with 50 mL(STP)/min of a 10 vol% H_2/N_2 mixture. Ethanol and water were feed independently into the pre-heater by means of syringe pumps (Becton–Dickinson) before mixing with carrier N_2. The samples in reduced form were tested in steam reforming of ethanol (H_2O/EtOH(mol/mol) = 3.0, N_2 = 44% vol) under a GHSV = 24,487 h^{-1} at atmospheric pressure and 773 K maintaining the reaction for 24 h in order to check if there was any deactivation of the catalysts. The above reaction conditions favours coke formation and allows to know the evolution of the catalyst towards carbon poisoning, that is the main phenomenon responsible for catalysts deactivation in this reaction, in a short period of time (24 h). The reaction products were analysed *on line* by GC with TCD (Varian chromatograph Model Star 3400 CX) equipped with Porapack Q (CO_2, C_2H_6, C_2H_4, water, acetaldehyde, ethanol, acetone, acetic acid, diethyl ether, ethyl acetate and crotonaldehyde) and molecular sieve 5A (H_2, O_2, N_2, CO) packed columns connected in series, using He as carrier gas.

3. Results

3.1. Characterization of fresh catalysts

3.1.1. Chemical composition and textural properties

Table 1 shows the chemical composition, expressed as oxide weight percentages, of calcined catalysts obtained from ICP-AES analyses. For all samples, the chemical compositions measured were close to the target loading. The textural properties (S_{BET}, pore diameter and pore volume) of the catalysts and supports are summarized in Table 2. For the sake of a valid comparison, the N_2 adsorption–desorption data were normalized to unit weight of Al_2O_3 carrier. Textural data in Table 2 show that the surface area of Al_2O_3 was almost constant after the incorporation of lanthanum to the bare Al_2O_3. This is not surprising because lanthanum ions form an atomic dispersed layer on alumina for loadings up to 8.5 μmol La/m^2 [10].

Table 2
Textural properties of calcined supports and catalysts as measured by N_2 adsorption–desorption isotherms at 77 K

	S_{BET} ($m^2/g_{Al_2O_3}$)	V_{pore} ($cm^3/g_{Al_2O_3}$)	D_{pore} (nm)
A	212	0.82	15.5
A3L	218	0.81	14.9
A6L	225	0.80	14.3
A15L	209	0.77	14.7
Ni/A	207	0.77	14.8
Ni/A3L	217	0.77	14.3
Ni/A6L	224	0.77	13.8
Ni/A15L	217	0.72	13.2

The incorporation of nickel to the supports did not change the textural properties of bare supports. The mean pore diameter after nickel deposition decreased slightly indicating some filling of pores by nickel species that does not significantly change the catalysts accessibility respect to unloaded supports.

3.1.2. FTIR of chemisorbed pyridine

To examine the strength of acid sites on supports, Fig. 1 shows the FTIR spectra of adsorbed pyridine on supports at room temperature after evacuation at 423, 523 and 623 K. Spectra of all samples show absorption bands at 1450, 1492, 1578 and 1620 cm^{-1} characteristic of vibrations associated to pyridine adsorbed on Lewis acid sites [11]. It was not detected absorption bands at 1540 cm^{-1}, characteristics of pyridine molecules adsorbed on Brønsted acid sites. The intensity of the strong band at 1445–1455 cm^{-1}, assigned to υ_{19b} vibration mode of pyridine, is proportional to the total number of Lewis acid sites while the wave number of the bands detected in the 1600–1620 cm^{-1} region, associated to the υ_{8a} vibration mode of pyridine, gives information about the strength of the Lewis acid sites on the surface.

The bare Al_2O_3 support degassed at 423 K (Fig. 1A) shows two contributions at 1615 and 1622 cm^{-1}. Respect to bare alumina, lanthanum containing Al_2O_3 supports (A3L, A6L and A15L, Fig. 1A) gave an additional band at 1600 cm^{-1} whose intensity increase with the increase in the lanthanum loading. Taking into account the fact that the wave number of bands at 1600–1620 cm^{-1} is very sensitive to the strength of the Lewis acid sites, it appears that addition of lanthanum to Al_2O_3 converts its original Lewis acid sites to another kind of Lewis acid sites. It has been suggested that La atoms titrate the original Lewis acid sites of Al_2O_3 via interaction of La atoms with the coordinatively unsaturated Al atoms through oxygen atoms [12]. As it is observed in Fig. 1B and C, after evacuation at 523 and 623 K supports with lanthanum showed a lower relative intensity of the band at 1600 cm^{-1} respect to 1614–1622 cm^{-1} bands than the variation observed in the case of bare Al_2O_3. This decrease is proportional to lanthanum loading indicating, therefore, the weaker acid strengths of the acid sites related to lanthanum species respect to those associated to original alumina surface.

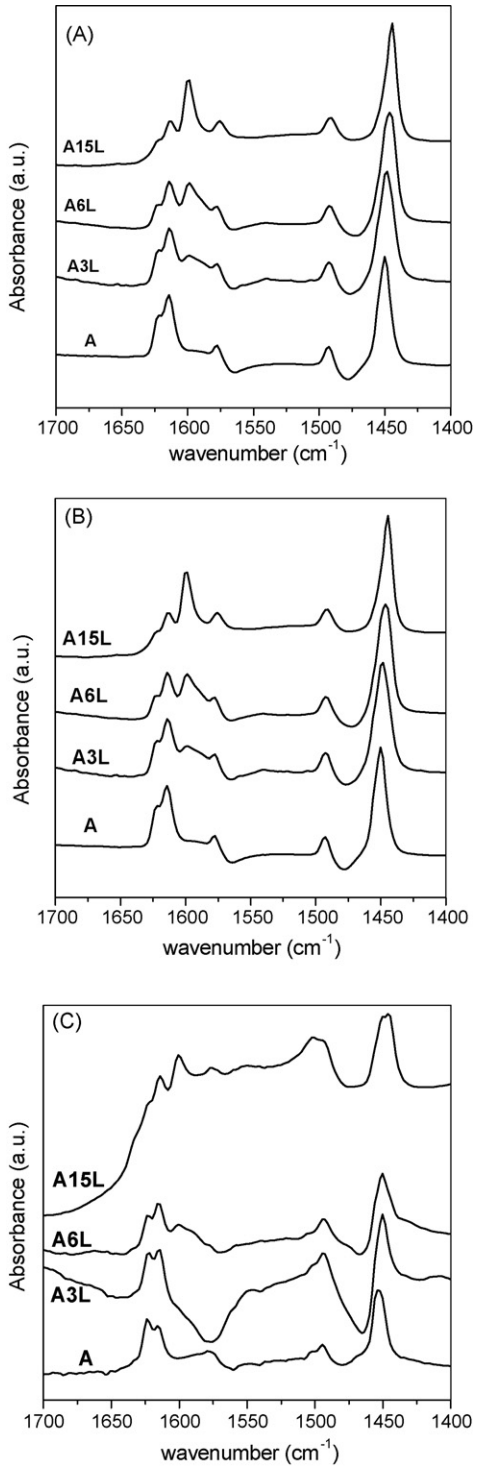

Fig. 1. FTIR spectra of adsorbed pyridine at 298 K on calcined supports and evacuated at: 423 K (A), 523 K (B) and 623 K (C).

3.1.3. X-ray diffraction (XRD)

XRD patterns of the fresh supports (not shown here) only exhibited the characteristic peaks of poorly crystalline γ-Al_2O_3 (at 46.8° and 66.7 JCPDS 86-1410). In no case diffraction peaks corresponding to crystalline species of either La_2O_3, $La(OH)_3$, $La_2(CO)_2O_2$ or $LaAlO_3$ phases were detected in lanthanum containing supports.

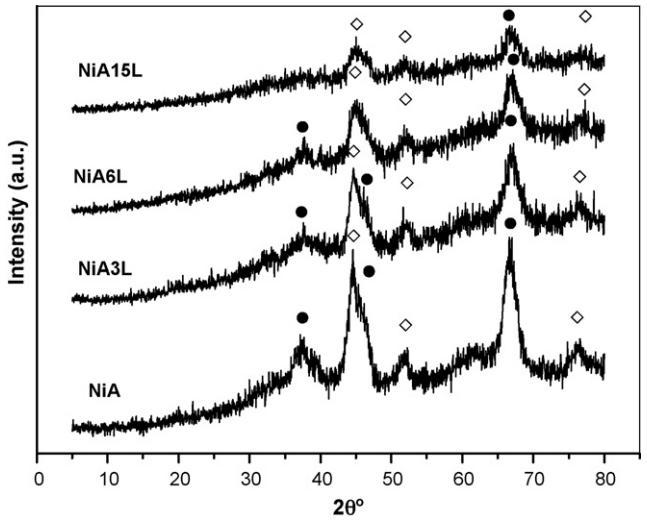

Fig. 2. XRD patterns of Ni catalysts after reduction under H_2/N_2 flow at 923 K ((◇) Ni^0, (●) Al_2O_3).

The X-ray diffraction patterns of reduced catalysts after treatment under H_2/N_2 (1/9 vol, 100 mL/min at 923 K for 2 h) are displayed in Fig. 2. XRD patterns of reduced catalysts in Fig. 1 show the diffraction line corresponding to the (2 0 0) reflection of Ni^0 phase (at 2θ angle of 51.8° JCPD 04-850). The low XRD reflections corresponding to metallic Ni phases may lead to some inaccuracies in the determination of absolute crystalline sizes. Nevertheless, quantitative estimation of crystallite sizes by applying the Scherrer equation, after a careful mathematical treatment of diffraction patterns, allows achieving the accuracy degree necessary for comparative purposes. Taking this fact in mind, the quantitative estimation of crystallite sizes of Ni^0 showed in Table 3 indicates the lower crystal size of metallic Ni with the increase in La loading.

3.1.4. Temperature-programmed reduction (TPR)

The TPR of bare supports (results not shown here) showed a broad and very low consumption of hydrogen between 700 and 1200 K for samples containing La. Taking into account the irreducible nature of lanthanum oxides, additional TPR-MS experiments were performed on supports indicating that the observed H_2 uptake during TPR corresponded to decomposition of some impurities adsorbed on surface. Analysis of species generated during TPR indicates that impurities are composed mainly of carbonates derived from the easy carbonation of surface La by exposure to ambient atmosphere.

The TPR profiles corresponding to Ni catalysts deposited on La–Al_2O_3 supports are depicted in Fig. 3. Quantification of

Table 3
Average size of NiO and Ni^0 crystalline particles from XRD data of calcined, reduced and used Ni catalysts

	Calcined NiO (nm)	Reduced Ni^0 (nm)	Used Ni^0 (nm)
Ni/A	10	7	15
Ni/A3L	8	7	10
Ni/A6L	5	6	11
Ni/A15L	4	5	4

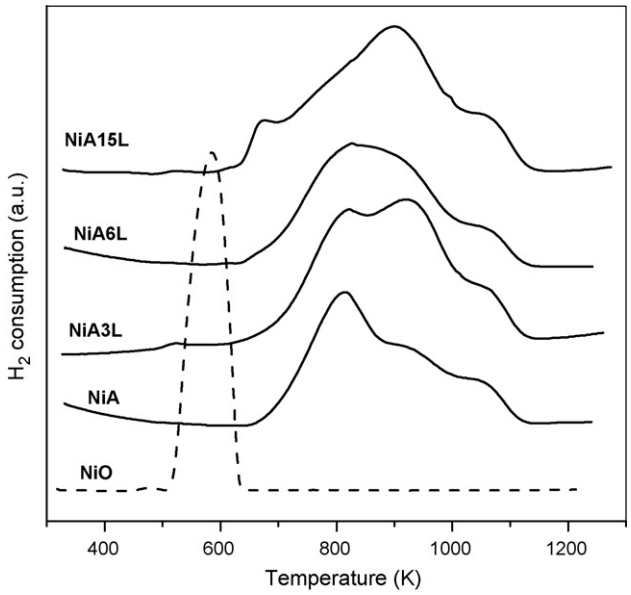

Fig. 3. Temperature-programmed reduction profiles of Ni catalysts (10% vol H_2/Ar, heating rate 10 K/min).

Table 4
Quantitative TPR data of calcined catalysts

	NiO–Al	Surface $NiAl_2O_4$	$NiAl_2O_4$
Ni/A	812 K, 65%	901 K, 24%	1053 K, 11%
Ni/A3L	803 K, 39%	931 K, 51%	1057 K, 10%
Ni/A6L	795 K, 48%	912 K, 44%	1054 K, 18%
Ni/A15L	758 K, 24%	923 K, 67%	1069 K, 9%

TPR data are summarized in Table 4. TPR data showed differences in the relative proportion of nickel species depending on the support used to disperse the nickel entities. As it is observed in Fig. 3, all calcined catalysts exhibited a broad reduction peak in the 650–1150 K range, which could be deconvoluted into three components at reduction temperatures of 818, 942 and 1041 K. According to literature studies, the reduction peak at 818 K is attributed to reduction of NiO species with weak interaction with alumina support [13],while the reduction peaks appearing at higher temperatures are related to the reduction of highly dispersed non-stoichiometric amorphous nickel aluminate spinels and to a diluted $NiAl_2O_4$-like phase, respectively [14]. From results presented in Fig. 3 and Table 4 it is observed that the incorporation of lanthanum to Al_2O_3 increases the proportion of highly dispersed nickel aluminate spinels (peak at 910–930 K) with concomitant decrease in the proportion of nickel with weak interaction with support (peak at 820 K). This experimental fact may be associated with the presence of surface species containing Ni, Al and La derived from a strong interaction of Ni with La ions.

3.1.5. X-ray photoelectron spectroscopy (XPS)

The binding energies of core electrons and the surface atomic ratios of the calcined and reduced catalysts are summarized in Table 5. For supports, La $3d_{5/2}$ peaks are centred at a binding energy of 835.7 eV. This BE is higher than the characteristic value for La_2O_3 (834.3 eV) and $LaAlO_3$ (833.8) [15,16] and can be assigned to well-dispersed lanthanum species on alumina [17]. The calculated La/Al XPS atomic ratio (Table 5) similar to the values corresponding to the bulk composition is indicative of a good diffusion at surface level of lanthanum ions into the alumina framework [17]. All calcined catalysts show the main line of Ni $2p_{3/2}$ level at 856.4 eV (Table 5). This binding energy was slightly higher than the value reported for pure NiO species (854.4 eV) and close to nickel aluminate (855.6 eV). Calculated XPS Ni/Al surface atomic ratios in Table 5 indicate differences in the relative metal exposure depending on the lanthanum loading added to Al_2O_3 and show an increase in the nickel surface concentration with the increase in the lanthanum loading on the Al_2O_3 substrate.

Table 5
Binding energies (eV) of core electrons and surface atomic ratios for Ni catalysts in calcined and reduced state

	Al 2p	La $3d_{5/2}$	Ni $2p_{3/2}$	La/Al	Ni/Al
Ni/A					
Calcined	74.5		856.5		0.11 (0.13)[a]
Reduced	74.5		856.4 (69.4%)		0.03
			852.7 (30.6%)		
Ni/A3L					
Calcined	74.5	835.8	856.1	0.015 (0.013)[a]	0.15 (0.14)
Reduced	74.5	835.8	855.9 (72%)		0.03
			854.1 (28%)		
Ni/A6L					
Calcined	74.5	835.8	856.2	0.028 (0.03)[a]	0.18 (0.15)
Reduced	74.5	835.5	856.1 (72.2%)		0.02
			851.8 (27.8%)		
Ni/A15L					
Calcined	74.5	835.8	856.3	0.082 (0.077)[a]	0.23 (0.15)
Reduced	74.5	835.4	856.2 (62.2%)		0.04
			851.8 (37.8%)		

[a] In parenthesis the value corresponding to bulk Ni/Al ratio.

Table 6
Hydrogen chemisorption results for reduced catalysts

	Dispersion (%)	Metal surface area (m^2/g)
Ni/A	6.0	3.1
Ni/A3L	5.5	2.8
Ni/A6L	8.4	4.3
Ni/A15L	8.2	4.2

The chemical state of catalysts surface after reduction in H_2 at 923 K was also investigated by XPS and the results are summarized in Table 5. Reduced catalysts showed binding energies characteristic of Ni^0 (852.6 eV) and Ni^{2+} ions in nickel aluminate entities (856.2 eV). As it can be observed in Table 5, it is clear that none of samples were completely reduced after the reduction protocol applied. This fact confirms the difficulties observed in TPR for the reduction of nickel with interactions with ions from the supports. After reduction, all catalysts showed surface Ni/Al ratios lower than nominal values (Table 5) indicating low metal dispersion and/or 'decoration' of metallic particles by dispersed species from support during the impregnation process. The XPS surface Ni concentrations (Table 5) did not match with the order of nickel dispersion derived from XRD (Table 3) and H_2 chemisorption (see next paragraph). Therefore, the lower XPS Ni surface concentration observed for reduced samples points to the important participation of dispersed entities with Al^{3+} and La^{3+} ions from the supports in the surface covering of metallic Ni particles.

3.1.6. H_2 pulse chemisorption

The amount of exposed nickel atoms in reduced catalysts, as determined by pulsed-H_2 chemisorption, is given in Table 6. As Table 6 shows, the dispersion degree of nickel on catalysts is relatively low as typically observed for high Ni content catalysts. Nevertheless higher metal exposition was found with the increase of lanthanum load on Al_2O_3 support.

3.2. Catalytic activity

The conversion of ethanol and the distribution of products for the steam reforming of ethanol over bare supports are presented in Table 7. These data indicate that ethanol was completely converted on bare Al_2O_3. Analysis of products show that the only product observed from the reforming of ethanol on Al_2O_3 was ethylene formed by dehydration of ethanol over the acidic sites of Al_2O_3. The conversion of ethanol over La–Al_2O_3 supports decreases slightly with the increase in the lanthanum loading. Analysis of products obtained over the La containing supports show an increase in the dehydrogenation/aldol condensation products (H_2, CO_2 and acetone) proportional to the increase in the lanthanum content on the support. These results indicate that lanthanum species in the support not only decreases the activity associated to acid sites of Al_2O_3 but also plays a role in the activity favouring the dehydrogenation/aldol condensation reactions that leads to the formation of H_2, CO_2 and acetone.

Fig. 4 shows the conversion of ethanol and the distribution of products for the steam reforming of ethanol over reduced Ni catalysts. When Ni is deposited on bare Al_2O_3 carrier, the reaction selectivity (Fig. 4A) differs strongly from that of the Al_2O_3 support (Table 7). Obviously nickel favours dehydrogenation of ethanol and subsequent C–C bond scission of acetaldehyde to CH_4 and CO. However these products were only observed in the first hours in reaction. The product selectivity changes along the reaction time in such a manner that C_2H_4, CO, CO_2 and H_2 are the only products at the end of the experiment (Fig. 4A). This product distribution indicates that the dominant reaction in the ethanol conversion over Ni/A catalyst was the ethanol dehydration to ethylene followed by its steam reforming on Ni phases that yields to CO, CO_2 and H_2. The sample with low lanthanum loading (Ni/A3L, Fig. 4B) presents a similar behavior to that observed on for the sample supported on bare Al_2O_3. However the catalyst with medium and high lanthanum loadings (Ni/A6L and Ni/A15L in Fig. 4C and D) present high initial capacity to break C–C bonds (absence of ethylene in products) and better stability that minimizes the changes in product distribution with time on stream previously observed for sample supported on bare alumina.

The enhancement in the stability of the Ni catalysts with the addition of lanthanum to Al_2O_3 observed in this study was also corroborate in additional long-term tests performed under conditions similar to those used in a fuel processor for hydrogen production (T = 923–973 K, H_2O/C = 3.8–4.8) observing for the NiA15L catalyst an activity and H_2 selectivity close to thermodynamic calculations without symptoms of deactivation for 100 h on stream.

3.3. Characterization of used catalysts

3.3.1. XRD

Diffraction patterns of used catalysts are displayed in Fig. 5. The diffraction patterns corresponding to used catalysts show,

Table 7
Ethanol conversion and product distribution for the steam reforming of ethanol over bare supports

	Conversion (mol%)	Product selectivity (mol%)[a]					
		H_2	CO_2	C_2H_4	CH_3–CHO	CH_3–CO–CH_3	CH_3–COOH
A	100	–	–	99.7	0.3	–	–
A3L	100	2.2	0.3	97.2	0.3	–	–
A6L	98.8	6.5	1.1	91.1	0.7	0.6	
A15L	75.4	26.0	5.7	58.3	1.3	2.4	3.5

[a] Gas phase, dry basis.

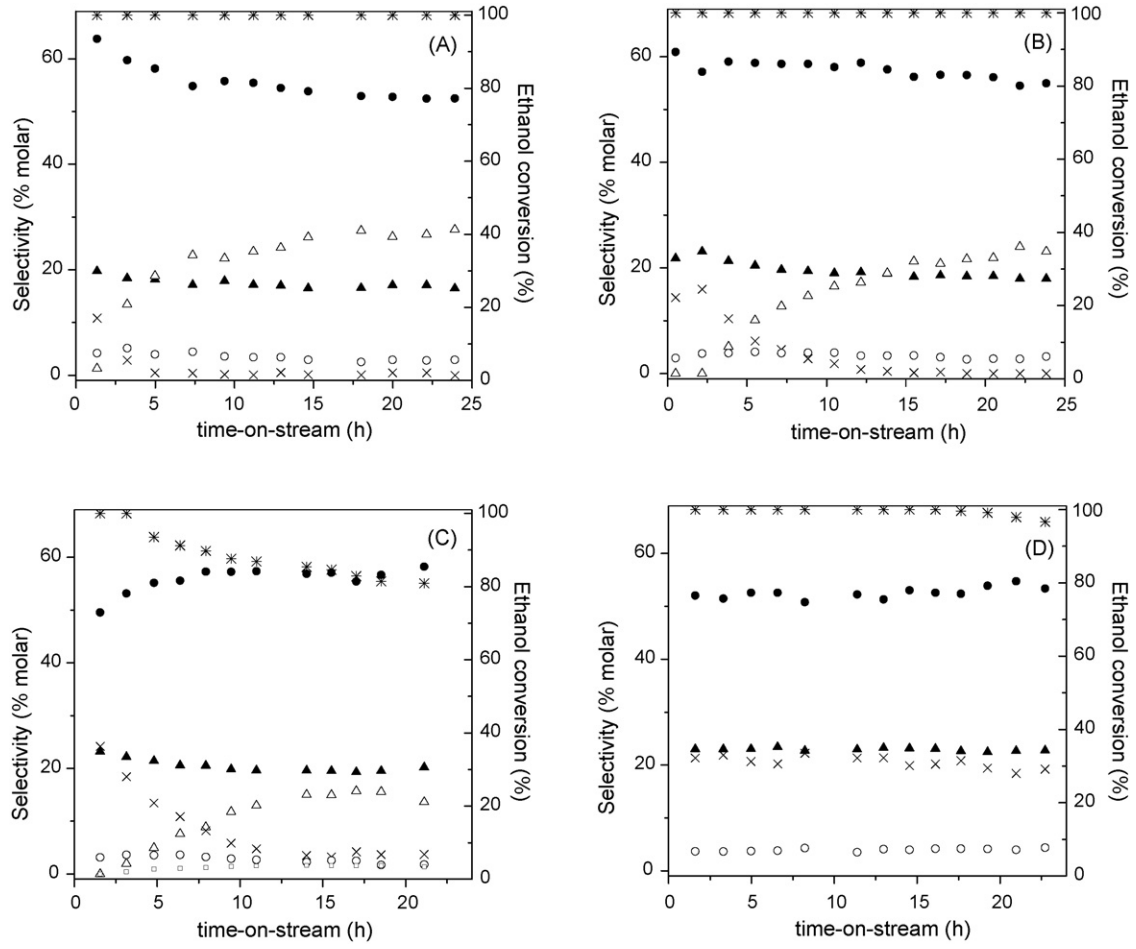

Fig. 4. Ethanol conversion ((ж)) and product distribution ((●) H_2, (▲)CO_2, (△) C_2H_4, (×) CH_4, (O) CO) during the steam reforming of ethanol over: Ni/A (A), Ni/A3L (B), Ni/A6L (C) and Ni/A15L (D) catalysts (T = 773 K, P = 0.1 MPa, GHSV = 24,500 h^{-1}).

additionally to reflections corresponding to Al_2O_3 and metallic Ni phases, diffraction peaks corresponding to crystalline forms of graphitic carbon at $2\theta = 26.2^\circ$ (JCPDS-75-1621). As observed in Fig. 5, the intensity of reflections associated to graphitic carbon decreases with lanthanum content in the supports. Quantitative estimation of crystalline domains of Ni in used samples by applying the Scherrer equation after carefully peak deconvolution (Table 3) indicates some degree of sintering of Ni^0 metal particles after reaction for Ni supported on bare Al_2O_3 (Ni/A). The sintering of nickel particles is less marked for the samples containing lanthanum, even absent in the sample with higher lanthanum load (Ni/A15L).

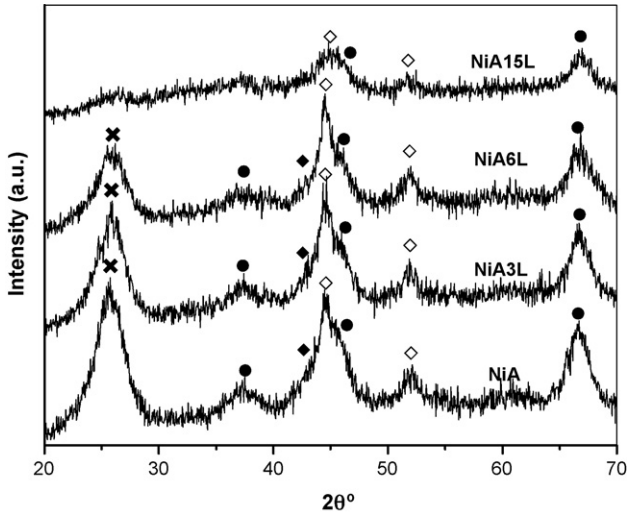

Fig. 5. XRD patterns of Ni catalysts after reaction ((●) Al_2O_3, (◇) Ni^0, (×) graphitic carbon).

3.3.2. Thermogravimetric analyses

Thermogravimetric analyses of the spent catalysts and supports were carried out to calculate the amount of carbonaceous residues retained in the catalysts after reaction by measuring the weight loss during its temperature-programmed oxidation under oxygen gas flow. Thermograms of used supports (not presented here) showed one slight weight loss within the range 650–750 K. The coke content corresponding to this weight loss (Table 8) were low for all supports and independent of the lanthanum loading in spite of the high activity shown by these samples.

The thermograms of used catalysts, presented in Fig. 6, can be divided into three different temperature regions: region I at temperatures lower than 573 K that can be ascribed to the loss

Table 8
Carbon deposition determined by thermogravimetry on supports and nickel catalysts used in the ethanol steam reforming reaction

	g C g^{-1} cat	mol C mol^{-1} Ni
A	0.042	
Ni/A	2.62	101.9
A3L	0.042	
Ni/A3L	2.22	86.4
A6L	0.039	
Ni/A6L	1.48	55.1
A15L	0.04	
Ni/A15L	0.42	16.6

of water and volatile species such as reactants, products and reaction intermediates, region II (573 K < T < 803 K) ascribed to filamentous coke associated to nickel particles [18] and region III (T > 803 K) ascribed to oxidation of coke deposits with different degree of graphitization [19]. The coke contents in used catalysts presented in Table 8 were calculated from the weight losses between 573 and 1100 K. Compared with bare supports, the amount of coke deposited on nickel catalysts was much higher indicating that the majority of coke was originating from dehydrogenation and polymerization reactions over nickel surfaces. As it is observed in Fig. 6, the coke deposited on Ni/A was in the form of both filamentous (773 K) and graphitic coke (872 K). For Ni/AL catalysts, the formation of carbon filaments is markedly suppressed as indicated by the lower relative intensity of the oxidation peak at 780 K. Quantification of coke contents in used Ni/AL catalysts (Table 8) show that the total amount of coke produced on these samples decreases markedly upon increasing La-loading in the Al_2O_3 support.

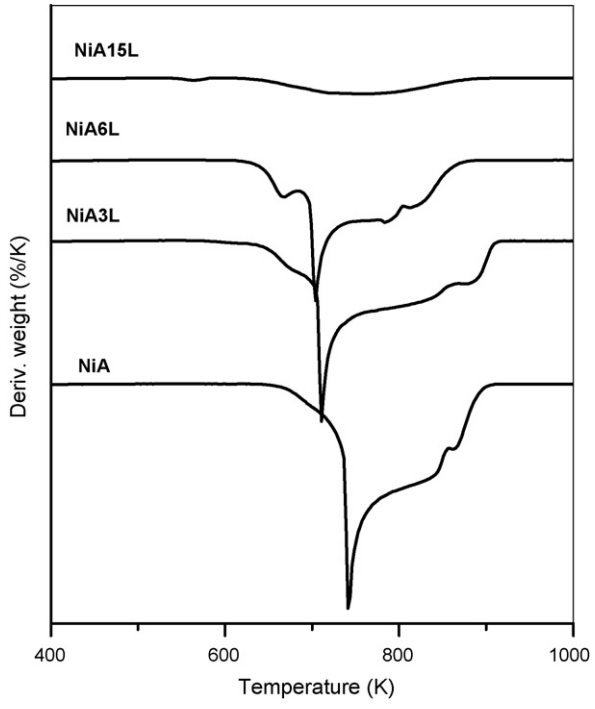

Fig. 6. Thermograms corresponding to the temperature-programmed oxidation of Ni catalysts used in the reforming of ethanol.

4. Discussion

According to the mechanism described for ethanol steam reforming, both metal and support play an essential role in the catalytic behavior of supported Ni catalysts [20]. The acidic properties of the supports may directly affect the activity of the catalyst since ethanol could adsorb on Al_2O_3 and reacts toward ethylene by means of dehydration reactions catalyzed by pairs of acidic sites [21]. Therefore, the lower ethylene selectivity observed in the ethanol reforming over supports with higher lanthanum content (Table 7) might be related to a decrease in surface acidity of Al_2O_3 derived from the addition of lanthanum (Fig. 1). However as Fig. 7 shows, the sequence of surface acidity determined from the integration of FTIR pyridine absorption band at 1450 cm^{-1} does not correlate with the selectivity to ethylene obtained over the supports. This observation points out that the modification of the original acidity of Al_2O_3 by the addition of lanthanum was not the only reason that influences on the observed behavior of the supports in the steam reforming of ethanol. Pure La_2O_3 have shown activity in the reforming of ethanol promoting the dehydrogenation/aldol condensation reactions of ethanol [20]. Taking this fact into account, the direct relationship found between the selectivity to the products directly associated to lanthanum oxides activity (H_2, CO_2 and acetone) and the lanthanum content on supports (Table 7) indicates that the observed change in the product selectivity with the increase in lanthanum load on supports may be more probably related with a direct participation of lanthanum species in the reaction scheme promoting the dehydrogenation/aldol condensation pathways.

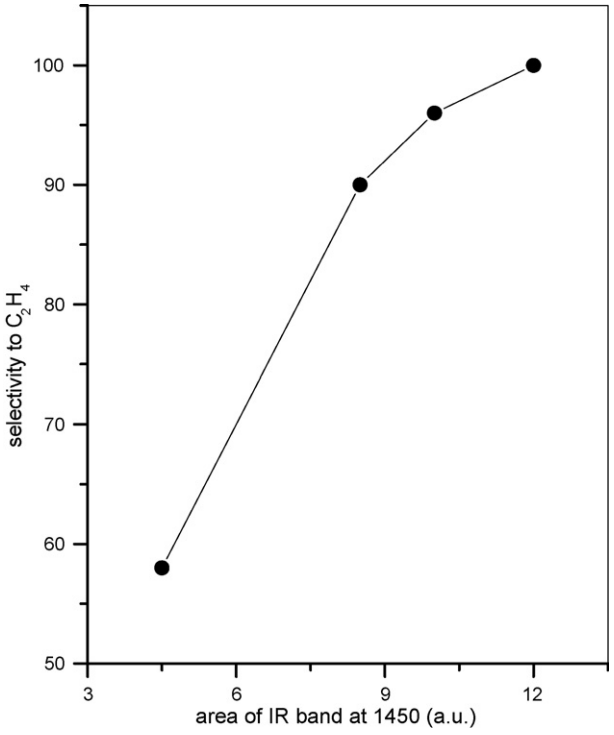

Fig. 7. Selectivity to ethylene in the ethanol steam reforming over supports vs. number of acidic sites derived from intensity of FTIR pyridine adsorption band at 1450 cm^{-1}.

The presence of nickel is an important parameter for the catalytic performance taking into account that nickel metal activates the organic molecule, by means of O–H, C–C and C–H bond breaking, and promotes the reaction between the organic fragments with the OH groups from the water reagent [22]. Analysis of initial product distribution observed in the reforming of ethanol over the Ni catalysts (H_2, CO_2, CH_4 and CO) indicates that reaction over the catalysts started with a very high dehydrogenating and C–C bond breaking capacities. When comparing the Ni surface concentration sequence obtained by XRD and H_2 chemisorption (Ni/A15L ≈ Ni/A6L > Ni/A3L ≈ Ni/A) with the initial selectivity to C_1 products (CH_4, CO and CO_2) it is evident that initial Ni dispersion influences on the initial capacity of the catalysts to break C–C bonds. However, the evolution of reaction products with reaction time (Fig. 5) is indicative of a progressive modification of the initial characteristics of catalyst surfaces. Catalysts modification was quick and significant on Ni/A whereas for Ni/AL catalysts the evolution was more moderate. The progressive appearance of ethylene with time on stream is indicative of a loss in the initial capacity of catalysts to transform ethylene into H_2, CH_4 and carbon oxides by means of steam reforming reactions [23], hydrogenolysis reactions or dehydrogenation/polymerization processes. The growth of carbon filaments on catalysts surfaces is believed to be responsible for the observed changes in product selectivities with reaction time. This variation, characterized by the loss in the transformation capacity of ethylene, may be related with the leaving of nickel particles from the support origin of ethylene production. Significant amounts of filamentous carbon covering nickel particles were observed on Ni/A while for catalysts with lanthanum in the supports the formation of carbon filaments was markedly suppressed (Fig. 6 and Table 8). Taking into account the easy dehydrogenation of ethylene to produce coke, one of the reasons to explain the differences on coke production may arise from the different capacity of the supports to generate ethylene. However the absence of a linear relationship between the selectivity to ethylene obtained over the supports (Table 7) and the amount of coke deposited over Ni catalysts (Table 8) indicates that apart of the capacity of support to generate ethylene there were another factors that influences on the coke deposition over the catalysts surfaces. In this sense the observed increase in the selectivity of C_2H_4 with concomitant decrease in CH_4 selectivity with time on stream (Fig. 4) is indicative of the importance of the reaction of hydrogenolysis of ethylene to methane on nickel surfaces as a competitive process with ethylene dehydrogenation that leads to coke deposition on metal surfaces. It is know that both the size and exposition of step edges on nickel particles plays an important role in the selectivity of dehydrogenation and hydrogenolysis reactions of ethylene on Ni surfaces [24]. In this sense the interaction of Ni atoms with elements that block the step sites, more reactive to ethylene dehydrogenation, is suggested to prevent coke deposition on catalysts applied to dehydrogenation of ethylene. TPR and XPS characterization over Ni catalysts deposited on La–Al_2O_3 carriers showed a closer interaction between lanthanum and Ni phases, lanthanum entities on top of metallic nickel crystallites, upon increase La-loading in the support. The close contact between Ni and La atoms may increase the blocking of Ni sites reactive to ethylene dehydrogenation that may explain the lower carbon filament formation observed on these samples responsible, as suggested previously, of the better stability of these catalysts for the steam reforming of ethanol. Apart of the possible participation of the lanthanum atoms in the blocking of Ni sites active for ethylene dehydrogenation, the close contact between Ni and lanthanum phases may also prevent coke deposition on catalysts by means of formation of lanthanum oxycarbonates intermediates that enhance the gasification of carbon precursors from hydrocarbon fragments (CH_x and carbon atoms) on the nickel surfaces [1].

5. Conclusions

Steam reforming of ethanol over nickel catalysts supported on Al_2O_3 with different lanthanum loading was investigated with respect to the structural and morphological characteristics of the dispersed metallic phase and the supports. Incorporation of lanthanum to Al_2O_3 support clearly improves the stability of nickel catalysts during the steam reforming of ethanol. The characterization of supports indicates that lanthanum incorporates to Al_2O_3 in the form a two-dimensional highly dispersed entities that neutralizes part of the original acidity of Al_2O_3. Modification of surface characteristics of Al_2O_3 with lanthanum improves the dispersion and stability of nickel metallic phases. Difference in catalyst stability observed for La-loaded catalysts respect to catalyst supported on bare Al_2O_3 was proposed to be related with the decreasing in the coke formation responsible of catalyst deactivation. The lower coke formation associated with the presence of lanthanum in the supports was related with the direct assistance of lanthanum lowering the capacity of nickel particles to dehydrogenate ethylene and/or increasing the participation in the gasification of carbon precursors by means of lanthanum oxycarbonates intermediates.

Acknowledgments

The authors thank financial support to Ministerio de Educación y Ciencia of Spain (Project MAT2003-08348-C04-01). M.C.S.S. acknowledges the Comunidad de Madrid for a predoctoral grant. R.M.N acknowledges the Ministerio de Educación y Ciencia for a Ramon y Cajal research program.

References

[1] A.N. Fatsikostas, D.I. Kondarides, X.E. Verykios, Catal. Today 75 (2002) 145.
[2] J. Llorca, N. Homs, J. Sales, P. Ramirez de la Piscina, J. Catal. 209 (2002) 306.
[3] M.S. Batista, R.K.S. Santos, E.M. Assaf, J.M. Assaf, E.A. Ticianelli, J. Power Sources 134 (2004) 27.
[4] F. Mariño, M. Boveri, G. Baronetti, M. Laborde, Int. J. Hydr. Energy 26 (7) (2001) 665.
[5] J.P. Breen, R. Burch, H.M. Coleman, Appl. Catal. B: Environ. 39 (2002) 65.
[6] D.K. Liguras, D.I. Kondarides, X.E. Verykios, Appl. Catal. B: Environ. 43 (4) (2003) 345.

[7] V. Fierro, O. Akdim, C. Mirodatos, Green Chem. 5 (1) (2003) 20.
[8] R.M. Navarro, M.C. Alvarez-Galván, M.C. Sanchez-Sanchez, F. Rosa, J.L.G. Fierro, Appl. Catal. B: Environ. 55 (4) (2005) 229.
[9] A.N. Fatsikostas, D.I. Kondarides, X.E. Verykios, Chem. Commun. 9 (2001) 851.
[10] M. Bettman, R.E. Chase, K. Otto, W.H. Weber, J. Catal. 117 (1989) 447.
[11] J.A. Wang, X. Bokhimi, O. Novaro, Y. Lopez, T. Tzompantzi, R. Gomez, J. Navarrete, M.E. Llanos, J.E. Lopez-Salinas, J. Mol. Catal. A: Chem. 137 (1999) 239.
[12] T. Yamamoto, T. Hatsui, T. Matsuyama, T. Tanaka, T. Funabiki, Chem. Mater. 15 (2003) 4830.
[13] J.T. Richardson, M.V. Twigg, Appl. Catal. A: Gen. 167 (1) (1998) 57.
[14] B. Scheffer, P. Molhoek, J.A. Moulijn, Appl. Catal. 46 (1989) 11.
[15] Y. Chen, Y. Liu, G. Niu, Z. Yang, M. Bian, A. He, Appl. Catal. A: Gen. 205 (1–2) (2001) 159.
[16] L.P. Haack, J.E. de Vries, K. Otto, M.S. Chatta, Appl. Catal. A: Gen. 82 (2) (1992) 199.
[17] J.S. Ledford, M. Houalla, M. Proctor, D.M. Hercules, L. Petrakis, J. Phys. Chem. 93 (18) (1989) 6770.
[18] S. Wang, G.Q.M. Lu, Appl. Catal. B: Environ. 16 (3) (1998) 267.
[19] S. Natesakhawat, R.B. Watson, X. Wang, U.S. Ozkan, J. Catal. 234 (2) (2005) 496.
[20] A. Fatsikostas, X.W. Verykios, J. Catal. 225 (2) (2004) 439.
[21] J.I. Di Cosino, U.K. Diez, M. Xu, E. Iglesia, R. Apesteguia, J. Catal. 178 (1998) 499.
[22] S.M. Gates, J.N. Russell, J.T. Yates, Surf. Sci. 171 (1) (1986) 111.
[23] J. Comas, F. Mariño, M. Laborde, N. Amadeo, Chem. Eng. J. 98 (2004) 61.
[24] R.T. Vang, K. Honkala, S. Dahl, E.K. Vestergaard, J. Schandt, E. Laegsgaard, B.S. Clausen, J.K. Norskov, F. Besenbacher, Surf. Sci. 600 (2006) 66.